Research Article | Vol. 29, No. 16 / 2 August 2021 / Optics Express 25270
Optics EXPRESS

Terahertz vortex beam generator based on bound states in the continuum

TaiRong Bai,[1] Qian Li,[1] YiQing Wang,[1] YiFan Chen,[1] Zheng-Da Hu,[1] and Jicheng Wang[1,2,*]

[1]School of Science, Jiangsu Provincial Research Center of Light Industrial Optoelectronic Engineering and Technology, Jiangnan University, Wuxi, 214122, China
[2]State Key Laboratory of Applied Optics, Changchun Institute of Optics, Fine Mechanics and Physics, Chinese Academy of Sciences, Changchun, 130033, China
*jcwang@jiangnan.edu.cn

Abstract: Vortex beams are playing an increasingly crucial role in wireless optical communications. Traditional vortex beam generators based on spiral phase plates and metasurfaces have a geometric center in real space, which limit their convenience in practical applications. In this work, we propose that the creation of a vortex beam can be achieved by using the bound state in the continuum (BIC) supported by a photonic crystal slab structure. Theoretical analysis shows that the proposed structure can be used as a kind of "momentum-space resonators" and thus can generate vortex beams. Moreover, higher-order vortex beams can also be achieved by changing the symmetry of photonic crystal slab, thus paving the way for the application of vortex beams in the fields of quantum information processing and micro optical micromanipulation.

1. Introduction

Optical vortex (OV) with phase singularity and helical wavefront is derived from the Helmholtz equation. Theoretical analysis shows that the phase of the wavefront at this phase singularity is not determined, and its amplitude is also zero [1,2]. The discovery of OV has made people realize that there is another special degree of freedom——orbital angular momentum (OAM), so vortex beams are also called OAM beams [3,4]. Since a vortex beam has the characteristics of hollowness, diffraction-resistant and quantized OAM, it is used in the fields of particle manipulation [5,6], large-scale wireless optical communication with high channel capacity [7–9], quantum information processing [10–12] and so on.

The typical vortex beam generation method mainly resorts to laser resonators [12]. However, this method not only requires high accuracy of axial symmetry of the resonator, but also is lack of stability. To this end, optical vortex generators based on spiral phase plates [13,14] and phased antenna arrays have been proposed [15]. These structures have solved the problem of vortex beam stability. However, due to the limitation of devices thickness and feed-network arrangements, when the operating wavelength is close to terahertz range, neither of these structures can be made into compact and integrated devices. In recent years, with the rapid development of metasurfaces [16–18], it has become possible to create the integrated vortex beam generators [19–23]. In addition, lots of researchers have made great efforts on finding a new way to generate vortex beam, therefore, many vortex beam generators based on momentum space polarization were produced recently [24,25]. However, this type of structures still has a geometric center in real space, which poses challenges in beam alignment, and the precise design of each unit cell brings difficulties to the fabrication of the device.

In this paper, we propose a terahertz vortex beam generator based on a photonic crystal slab structure. Unlike the traditional vortex beam generators, this structure does not have the vortex configuration in real space. However, through numerical simulation, we find that it indeed has vortex topological behavior in the momentum space. It is this characteristic that enables it to be

#431814 https://doi.org/10.1364/OE.431814
Journal © 2021 Received 19 May 2021; revised 15 Jul 2021; accepted 19 Jul 2021; published 23 Jul 2021

Optics EXPRESS

used as a vortex beam generator. By calculating its band structure and radiative quality factor, the BIC located at the **Γ** point of momentum space has been found, and the radiation mode around BIC in the far field has certain states of polarizations (SOPs), which presents a winding configuration around BIC. Due to the conjugate relationship between real space and momentum space, the vortex configuration in the momentum space can also induce the geometric phase so that OV can be generated. In addition, we also find that the topological charge carried by the excited OV is related to the topological charge of the BIC. Therefore, higher-order vortex beams can be also achieved by only changing the symmetry and structure parameters of the photonic crystal slab. Compared with the previous devices, the structure we propose here presents a periodic distribution in real space, which does not have a strict geometric center. Therefore, it can solve the problems of beam alignment and difficulties in fabrication very well.

2. Analysis of photonic crystal structure and its band structure

Figure 1(a) shows the proposed photonic crystal slab structure which has C_{4v} symmetry. The structure is composed of a tetragonal lattice arrangement of holes on a perovskite substrate (refractive index n_1=2.7), while the entire material is placed in the environment of refractive index n_2=1.5. The period of lattice is p=92.8μm, the radius of hole is r=34μm, and the thickness of slab is d=72.914μm. Since the proposed structure is up-down symmetric, only half of the slab need to be computed in the simulation model. And to ensure that the far-field polarization field is accurate enough, a thick enough air layer with a perfectly matched layer on the top is covered on the slab. Although the proposed crystal structure has a two-dimensional periodicity, the electromagnetic field energy will radiate to the outside of the slab since the system is non-Hermitian. Therefore, three-dimensional modeling is adopted [25–28]. The band structure of the quasi-TE mode calculated by the COMSOL eigenfrequency solver under Floquet periodicity boundary condition is shown in Fig. 1(b). The dispersion curve specially marked by the thick purple solid line is of interest to us. In order to verify whether there is a BIC at the Γ point of k-space, we use the formula [29]:

$$Q = \omega_0/2\gamma \tag{1}$$

to calculate the quality factor corresponding to this band. Here, ω_0 and γ are the real and imaginary parts of the intrinsic frequency, respectively, and the imaginary part is related to the radiation loss. The calculation result is shown in Fig. 1(c). It can be seen that the quality factor of the dispersion curve at the k-space Γ point approaches infinity, which proves that the eigenmode corresponding to this point is a BIC. When the photonic crystal slab is at this optical singularity, the light field will be completely coupled in the slab, which is a typical field distribution at k-space Γ point, and when it deviates slightly from the BIC, it will show radiation to the outside of the slab. This feature can be seen from the Figs. 2(a) and 2(b) visually. On the other hand, starting from the symmetry of the crystal lattice can also explain this phenomenon. Since the calculated eigenmode is located above the light line, it will couple to the continuum of extended modes and usually appears as a resonance with finite lifetime, so there should be outward radiation loss. Nonetheless, at the Γ point, due to the mismatch between the symmetry mode inside the lattice and any external propagation mode, the eigenmode appears as a BIC with infinite lifetime [30,31].

In order to better understand how this type of photonic crystal slab structure with periodicity in real space generates OV, it is necessary to study the topological properties of the BIC by investigating the far-field SOPs of these resonant guided modes. Figure 3(a) shows the three-dimensional structure of the quasi-TE mode band structure of the photonic crystal, where the lowest band is the one we are interested in, which corresponds to the dispersion curve marked by the thick purple line in Fig. 1(b). Figure 3(b) shows the iso-frequency diagram of the band structure. It can be found that the iso-frequency lines near the BIC phase singularity are approximately circular, which indicates that the studied band structure has a parabolic

Optics EXPRESS

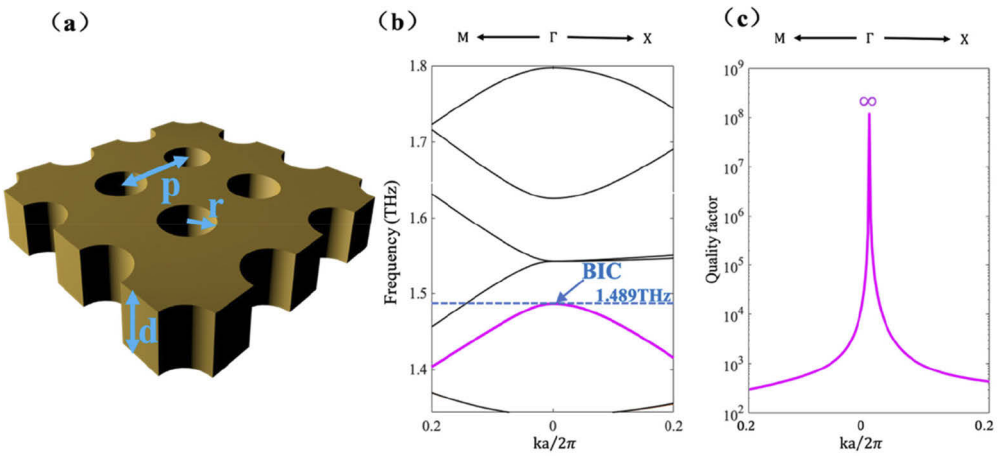

Fig. 1. (a) Schematic diagram of the photonic crystal slab structure. (b) The quasi-TE mode band structure of the proposed crystal structure, in which purple represents the dispersion curve of BIC at the Γ point, and the frequency corresponding to BIC is 1.489THz. (c) The quality factor distribution corresponding to the BIC band. It can be seen that the quality factor at the BIC point is close to infinity.

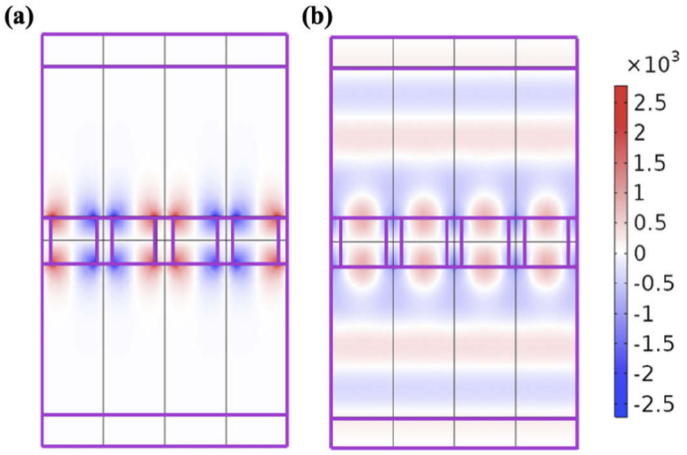

Fig. 2. (a) The optical field distribution of $|E_y|$ at the BIC point, which is bound to the photonic crystal slab without radiation loss. (b) The optical field distribution of $|E_y|$ deviating from the BIC point, at this situation the electromagnetic wave will radiate to the outside of the slab.

Optics EXPRESS

configuration and is advantageous to form a polarization vortex distribution in the momentum space.

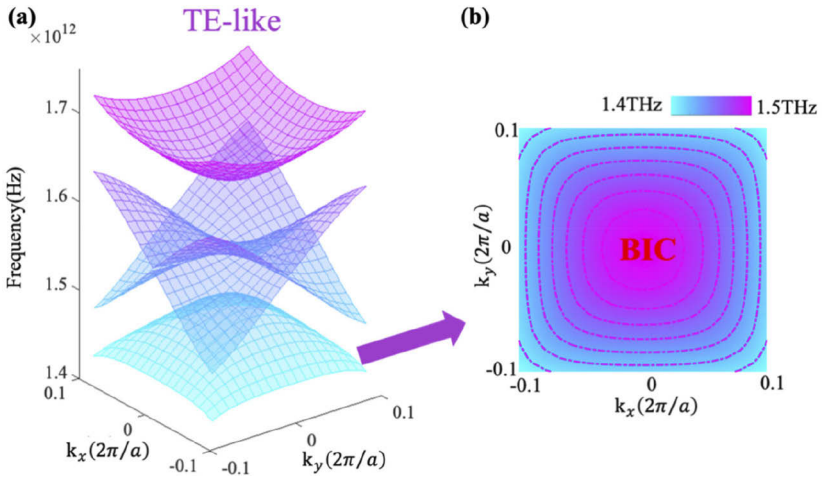

Fig. 3. (a) The three-dimensional structure of the band of the proposed photonic crystal slab, in which the lowest one is what we are concerning about. (b) The iso-frequency diagram of the studied band, where the iso-frequency line near the BIC point is near circular.

3. Topological properties of BIC and its vortex beam excitation effect

Then we use the Bloch theory [30,31] of photonic crystals to calculate the far-field SOPs corresponding to the dispersion curve under study. The expression of the resonance electric field is expressed as $\boldsymbol{E_k}(\boldsymbol{\rho}, z) = e^{i\boldsymbol{k}\cdot\boldsymbol{\rho}}\boldsymbol{u_k}(\boldsymbol{\rho}, z)$, where $\boldsymbol{k} = k_x\hat{x} + k_y\hat{y}$ is the two-dimensional in-plane wave vector, $\boldsymbol{\rho} = x\hat{x} + y\hat{y}$ is the in-plane radial coordinate, and $\boldsymbol{u_k}$ is the periodic function of $\boldsymbol{\rho}$ with period a. Inside the slab, the electric field is periodically modulated by the photonic crystal, while outside the slab, the electric field expression includes an evanescent wave whose amplitude decays exponentially. For the resonance mode above the light cone and the wavelength below the diffraction limit, the amplitude of the only propagating wave is the zero-order Fourier expansion coefficient of the electric field expression, expressed as $\boldsymbol{c}(\boldsymbol{k}) = c_x(\boldsymbol{k})\hat{x} + c_y(\boldsymbol{k})\hat{y}$, where

$$c_x(\boldsymbol{k}) = \hat{x} \cdot \langle \boldsymbol{u_k} \rangle \tag{2}$$

$$c_y(\boldsymbol{k}) = \hat{y} \cdot \langle \boldsymbol{u_k} \rangle \tag{3}$$

denote the polarization components in the x and y directions, respectively. The brackets represent the spatial average value of the electric field in the x-y plane of any unit in the far-field area outside the slab, and c(k) is called the polarization vector here.

For the BIC, due to the mismatch between its intrinsic mode and the propagation mode, the light field is completely coupled to the plate with the corresponding far-field polarization component $c_x = c_y = 0$. However, $c_x(\boldsymbol{k})$ and $c_y(\boldsymbol{k})$ are complex functions in general, and only the change of $\boldsymbol{k}(k_x, k_y)$ is not enough to guarantee the solution of $c_x = c_y = 0$. By contrast, for the photonic crystal structure we have proposed, since it satisfies the time reversal symmetry $\epsilon(\boldsymbol{\rho}) = \epsilon^*(\boldsymbol{\rho})$ and the space reversal symmetry $\epsilon(\boldsymbol{\rho}) = \epsilon(-\boldsymbol{\rho})$, the period of the electric field item

Optics EXPRESS

satisfies:

$$\boldsymbol{u}(\boldsymbol{\rho}) = \boldsymbol{u}^*(-\boldsymbol{\rho}) \tag{4}$$

In addition, the mirror symmetry in the z-direction makes the electric field added by a coefficient of ±1 under the action of the z-direction reflection operator, which gives rise to:

$$\boldsymbol{u}_{\boldsymbol{k}}(\boldsymbol{\rho}, z) = \boldsymbol{u}_{\boldsymbol{k}}(\boldsymbol{\rho}, -z) \tag{5}$$

Under the conditions of Eqs. (4) and (5), the polarization components $c_x(\boldsymbol{k})$ and $c_y(\boldsymbol{k})$ must be real or pure imaginary numbers, so the solution of $c_x = c_y = 0$ can be guaranteed. Figures 4(a) and 4(b) show the distribution of far-field polarization components in the momentum space calculated according to Eqs. (2) and (3) respectively. It can be seen that there is a nodal line representing $c_x = 0$ and $c_y = 0$, and the intersection of these two nodal lines is the BIC point, which is why the BIC is robust to crystal structure changes. On the other hand, the intersection of the two nodal lines will inevitably form a vortex configuration in the polarization vector field centered on the BIC, as shown in Fig. 4(c), Due to the fact that the eigenmode corresponding to the BIC has no radiation, its far-field SOP is undefined, and its topological charge can be defined as [30,31]:

$$q = (1/2\pi) \oint d\vec{k} \cdot \nabla_{\vec{k}} \psi(\vec{k}) \tag{6}$$

where $\psi(\vec{k}) = arg(c_x + ic_x)$ is the azimuth angle of the SOP (Fig. 4(d)), and the integration is performed counterclockwise along any closed curve around the BIC point with the calculation result −1.

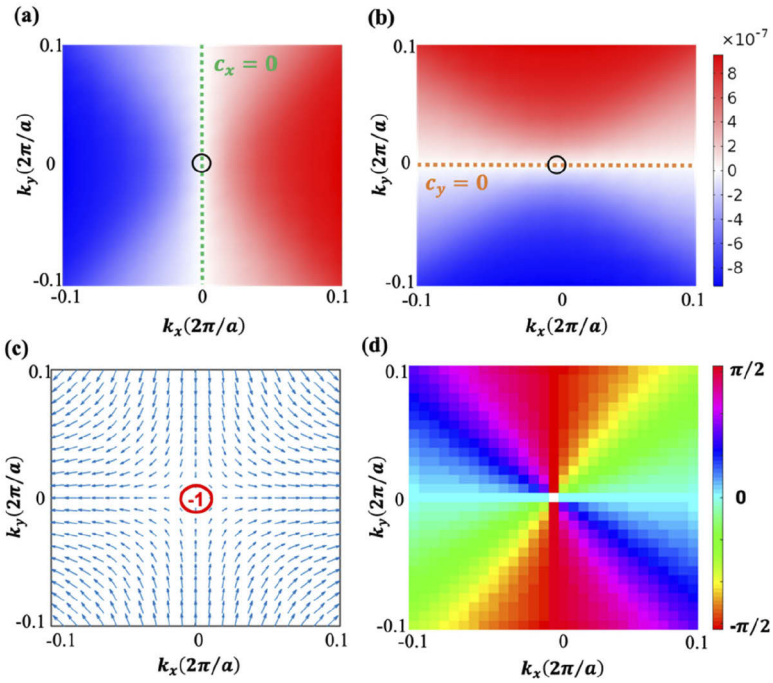

Fig. 4. (a) The x-polarization component distribution of the far field in momentum space. (b) The y-polarization component distribution of the far field in the momentum space. (c) The polarization vector distribution of the far field in the momentum space and the topological charge carried by the BIC. (d) The distribution of the azimuth angle of the far-field SOPs in the momentum space.

Optics EXPRESS

Now we consider that when a Gaussian beam with a specific in-plane wave vector $\vec{k}$ and a specific SOP is incident on the photonic crystal slab, it will interact with the resonance guide mode of the photonic crystal slab, in which case the expression of the transmitted light field is [32]:

$$\begin{aligned}\left|E_{out}\right\rangle = \frac{1}{2}\left[t_x\left(\vec{k}\right) + t_y\left(\vec{k}\right)\right]\left|E_{in}\right\rangle + \frac{1}{2}\left[t_x\left(\vec{k}\right) - t_y\left(\vec{k}\right)\right]e^{-2i\psi\left(\vec{k}\right)}\left\langle E_{in}|R|L\right\rangle \\ + \frac{1}{2}\left[t_x\left(\vec{k}\right) - t_y\left(\vec{k}\right)\right]e^{2i\psi\left(\vec{k}\right)}\left\langle E_{in}|L|R\right\rangle\end{aligned} \tag{7}$$

where $|E_{out}\rangle$ and $|E_{in}\rangle$ represent the Jones vectors of the outgoing and incident beams respectively; $t_x(\vec{k})$ and $t_y(\vec{k})$ represent the transmission factors associated with the in-plane wave vector $\vec{k}$ respectively. According to this formula, it can be known that when the incident beam has a left-handed circular SOP, the outgoing beam not only contains the same left-handed part as the incident beam, but also contains an additional cross-polarization state, which is related to the geometric phase. The existence of this term makes the outgoing beam have a spiral phase distribution to produce OV, according to the formula:

$$l = -2q \tag{8}$$

where the topological charge carried by vortex beam is 2. And this vortex beam with a specific topological charge can be represented by a Laguerre-Gaussian beam [15]:

$$E_{m,n}(r,z) = E_0\frac{w_0}{w(z)}e^{in\phi}\left(\frac{r}{w(z)}\right)^n L_m^n\left(\frac{2r^2}{w^2(z)}\right)exp\left(-\frac{r^2}{w^2(z)}\right)exp\left(-ikx - i\frac{kr^2}{2R(z)} + i\Psi_{m,n}(z)\right) \tag{9}$$

where w_0 is the beam waist radius (set to 2.14 mm here); k is the wave number; L_m^n is the generalized Laguerre polynomial with m (set to 0) and n (set to 2) representing the radial modulus and angle modulus respectively. The beam spot radius $w(z)$, the wavefront curvature radius R(z) and the phase function $\Psi_{m,n}(z)$ varying with the propagation distance z can be expressed as:

$$w(z) = w_0\sqrt{1 + \frac{z^2}{{z_0}^2}} \tag{10}$$

$$R(z) = z\left(1 + \frac{{z_0}^2}{z^2}\right) \tag{11}$$

$$\Psi_{m,n}(z) = (n + 2m + 1)arctan(z/z_0) \tag{12}$$

where $x_0 = \pi n_0 {w_0}^2/\lambda$ is the rayleigh range. Use the above formulas to calculate the propagation of the beam in the range of 0.5 to 53.5 mm, as shown in Figs. 5(a)–5(c). Here the formulas are set in MATLAB to compute pure mathematical or theoretical propagation of the vortex beam. It can be seen that the beam can still maintain a certain intensity after propagating a relatively long distance and has a good diffraction-resistant effect; also the hollow intensity distribution and spiral phase distribution are always maintained.

Subsequently,in order to get the numerical result of the vortex beam generated by proposed structure, we set up a 40×40 unit cell photonic crystal slab in the simulation, and use a focused circularly polarized Gaussian beam with its frequency of 1.45THz and the beam waist radius of 1.07 mm to be incident on the structure. It could be clearly seen from Fig. 3 and Fig. 4 that if the incident frequency (1.45THz) is marginally below frequency of the BIC phase singularity (1.489THz), its polarization vector distribution of the far field in the momentum space will have a spiral phase distribution, consequently, the outgoing beam become vortex beam. The propagation intensity and phase distribution of the generated beam in the range of 0.5 ~ 53.5mm are calculated, as shown in Figs. 6(a)–6(d). It can be found that both the electric field distribution

Optics EXPRESS

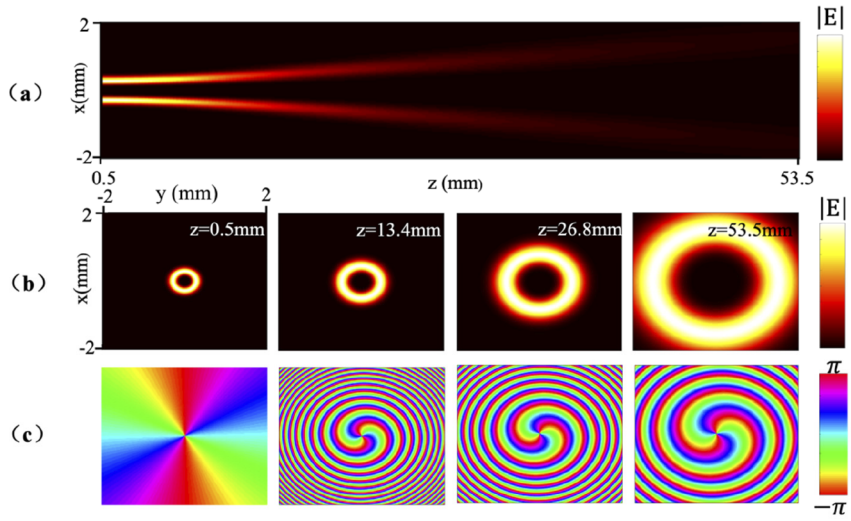

Fig. 5. Theoretical calculation results of propagation characteristics of high-order Laguerre-Gaussian beam $E_{0,2}$ along the z direction. (a) The electric field intensity distribution of the beam along z direction. (b) - (c) The transverse electric field intensity and phase distribution at z=0.5 mm, 13.4 mm, 26.8 mm and 53.5 mm.

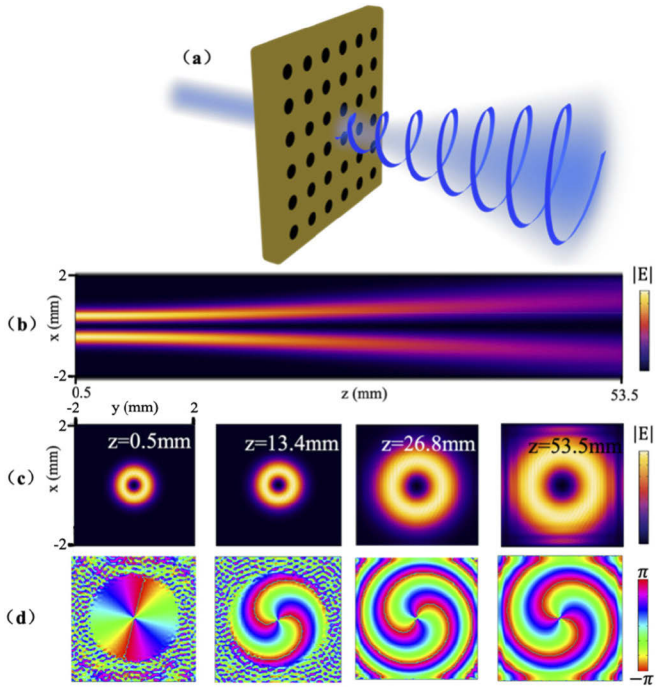

Fig. 6. (a) Schematic of the performance of the proposed photonic crystal slab structure, which generates a vortex beam carrying OAM in the case of circularly polarized Gaussian beam incident. (b) The electric field intensity distribution in the beam propagation direction (z direction). (c) - (d) Electric field distribution and phase distribution on cross-section at z=0.5 mm,13.4 mm,26.8 mm and 53.5 mm.

Optics EXPRESS

in the propagation direction and the phase distribution on the cross-section are basically consistent with the theoretical calculation results shown in Fig. 5. This calculation result verifies the correctness of the theory we put forward above, and further shows that the device can indeed be used as a high-performance OV generator.

As mentioned above, the topological charge of the beam generated by the photonic crystal slab structure is determined by the topological charge carried by the corresponding BIC, so higher-order vortex beams can be achieved by changing the symmetry of the structure. As shown in Fig. 7(a), the photonic crystal has the C_{6v} symmetry, with the period p=92.8μm, and the hole radius r=31.64μm. By calculating the band structure (Fig. 7(b)) and the quality factor (Fig. 7(c)), we find that the BIC is also located at the k-space Γ point. The far-field polarization vector distributions calculated by Eqs. (2) and (3) are shown in Fig. 7(d), and the topological charge carried by the BIC is calculated as −2 according to Eq. (6), which proves that the structure can generate a high-order vortex beam under the incidence of a circularly polarized Gaussian beam.

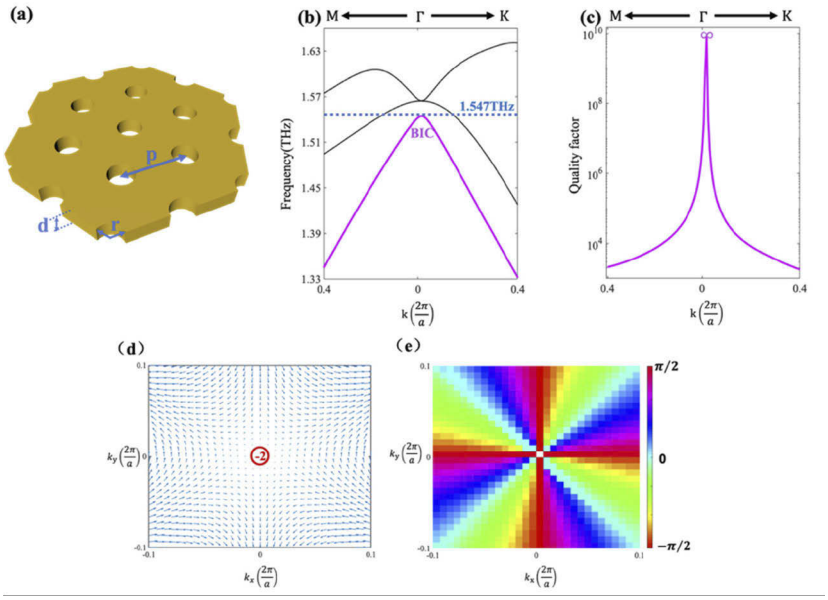

Fig. 7. (a) Schematic of the hexagonal lattice photonic crystal slab structure. (b) The proposed photonic crystal quasi-TE mode band diagram, in which the thick solid purple line is the dispersion curve under study, and the frequency corresponding to BIC is 1.547THz. (c) The quality factor distribution corresponding to the studied dispersion curve. (d) The distribution of the far-field polarization vector of the hexagonal lattice photonic crystal in the momentum space, and the topological charge carried by the BIC is −2. (e) The distribution of the azimuth angle of the far-field SOPs of the hexagonal lattice photonic crystal in the momentum space.

4. Conclusions

In conclusion, we have proposed a terahertz vortex beam generator based on BIC. By using the COMSOL software, the band diagrams are calculated, then the BIC is found. Moreover, we study the topological properties of the BIC and find that the SOPs of the resonant guided mode constitutes a winding configuration near the BIC and has a topological charge of −1. Therefore, when the circularly polarized Gaussian beam with a frequency slightly lower than that of the BIC frequency is incident on the photonic crystal device, it will interact with these resonant

Optics EXPRESS

guided modes to obtain the PB phase, which can excite an OAM beam. The topological charge of the beam is determined by that of the BIC. It is worth mentioning that the structure has a periodic distribution in the real space and does not have a strict geometric center, which displays significant advantages in fabrication and practical applications.

Funding. China Science and Technology Exchange Center (CB02-20); State Key Laboratory of Transient Optics and Photonics (SKLAO2020001A04); Jiangnan University (2020366Y); National Natural Science Foundation of China (11811530052).

Disclosures. The authors declare that there are no conflicts of interest related to this article.

Data availability. The data that support the findings of this study are available from the corresponding author upon reasonable request.

References

1. P. Coullet, L. Gil, and F. Rocca, "Optical vortices," Opt. Commun. **73**(5), 403–408 (1989).
2. L. Allen, M. Beijersbergen, R. Spreeuw, and J. Woerdman, "Orbital angular momentum of light and the transformation of Laguerre-Gaussian laser modes," Phys. Rev. A **45**(11), 8185–8189 (1992).
3. M. W. Beijersbergen, L. Allen, H. E. L. O. van der Veen, and J. P. Woerdman, "Astigmatic laser mode converters and transfer of orbital angular momentum," Opt. Commun. **96**(1-3), 123–132 (1993).
4. K. Y. Blikh, "Geometrical optics of beams with vortices: Berry phase and orbital angular momentum Hall effect," Phys. Rev. Lett. **97**(4), 043901 (2006).
5. M. Padgett and R. Bowman, "Tweezers with a twist," Nat. Photonics **5**(6), 343–348 (2011).
6. B. K. Singh, H. Nagar, Y. Roichman, and A. Arie, "Particle manipulation beyond the diffraction limit using structured super-oscillating light beams," Light: Sci. Appl. **6**(9), e17050 (2017).
7. J. Wang, J. Y. Yang, and I. M. Fazal, "Terabit free-space data transmission employing orbital angular momentum multiplexing," Nat. Photonics **6**(7), 488–496 (2012).
8. A. E. Willner, H. Huang, Y. Yan, Y. Ren, and S. Ashrafi, "Optical communications using orbital angular momentum beams," Adv. Opt. Photonics **7**(1), 66–106 (2015).
9. Z. W. Xie, T. Lei, F. Li, and H. D. Qiu, "Ultra-broadand on-chip twisted light emitter for optical communications," Light: Sci. Appl. **7**(4), 18001 (2018).
10. T. Stav, A. Faerman, E. Maguid, D. Oren, and V. Kleiner, "Quantum entanglement of the spin and orbital angular momentum of photons using metamaterials," Science **361**(6407), 1101–1104 (2018).
11. G. M. Terriza, J. P. Torres, and L. Torner, "Twisted photons," Nature Phys **3**(5), 305–310 (2007).
12. L. Chen, J. Lei, and J. Romero, "Quantum digital spiral imaging," Light: Sci. Appl. **3**(3), e153 (2014).
13. E. Brasselet, M. Malinauskas, A. Zukauskas, and S. Juodkazis, "Photopolymerized microscopic vortex beam generators: Precise delivery of optical orbital angular momentum," Appl. Phys. Lett. **97**(21), 211108 (2010).
14. V. S. Lyubopytov, A. P. Porfirev, and S. O. Gurbatov, "Simultaneous wavelength and orbital angular momentum demultiplexing using tunable MEMS-based Fabry-Perot filter," Opt. Express **25**(9), 9634–9646 (2017).
15. K. X. Cheng, Z. D. Hu, Y. Q. Wang, J. Ma, and J. C. Wang, "High-performance terahertz vortex beam generator based on square-split-ring metasurfaces," Opt. Lett. **45**(21), 6054–6057 (2020).
16. J. P. Fan, Y. Z. Cheng, and B. He, "High-efficiency ultrathin terahertz geometric metasurface for full-space wavefront manipulation at two frequencies," J. Phys. D: Appl. Phys. **54**(11), 115101 (2021).
17. J. P. Fan and Y. Z. Cheng, "Broadband high-efficiency cross-polarization conversion and multi-functional wavefront manipulation based on chiral structure metasurface for terahertz wave," J. Phys. D: Appl. Phys. **53**(2), 025109 (2020).
18. J. Y. Wang, J. P. Fan, H. Shu, C. Liu, and Y. Z. Cheng, "Efficiency-tunable terahertz focusing lens based on graphene metasurface," Opto-Electronic Engineering **48**(4), 200319 (2021).
19. B. He, J. Fan, Y. Cheng, F. Chen, H. Luo, and R. Gong, "Thermally tunable terahertz vortex beam generator based on an InSb metasurface," J. Opt. Soc. Am. B **38**(5), 1518–1524 (2021).
20. K. Huang, H. Liu, S. Restuccia, and M. Q. Mehmood, "Spiniform phase-encoded metagratings entangling arbitrary rarional-order orbital angular momentum," Light: Sci. Appl. **7**(3), 17156 (2018).
21. D. Hakobyan, H. Magallanes, G. Seniutinas, S. Juodkazis, and E. Brasselet, "Tailoring orbital angular momentum of light in the visible domain with metallic metasurfaces," Adv. Opt. Mater. **4**(2), 306–312 (2016).
22. J. X. Zhou, Y. C. Liu, Y. G. Ke, H. L. Luo, and S. C. Wen, "Generation of Airy vortex and Airy vector beams based on the modulation of dynamic and geometric phases," Opt. Lett. **40**(13), 3193–3196 (2015).
23. R. C. Devlin, A. Ambrosio, N. A. Rubin, J. Mueller, and F. Capasso, "Arbitrary spin-to-orbital angular momentum conversion of light," Science **358**(6365), 896–901 (2017).
24. Y. W. Zhang, A. Chen, W. Z. Liu, C. W. Hsu, B. Wang, F. Guan, X. H. Liu, L. Shi, L. Lu, and J. Zi, ""Observation of Polarization Vortices in Momentum Space," Phys. Rev. Lett. **120**(18), 186103 (2018).
25. B. Wang, W. Z. Liu, M. X. Zhao, J. J. Wang, Y. W. Zhang, A. Chen, F. Guan, X. H. Liu, L. Shi, and J. Zi, "Generating optical vortex beams by momentum-space polarization vortices centred at bound states in the continuum," Nat. Photonics **14**(10), 623–628 (2020).
26. M. Minkov, I. Williamson, M. Xiao, and S. H. Fan, "Zero-index bound states in the continuum," Phys. Rev. Lett. **121**(26), 263901 (2018).

Optics EXPRESS

27. W. M. Ye, Y. Gao, and J. L. Liu, "Singular points of polarizations in the momentum space of photonic crystal slabs," Phys. Rev. Lett. **124**(15), 153904 (2020).
28. C. Huang, C. Zhang, and Q. H. Song, "Ultrafast control of vortex microlasers," Science **367**(6481), 1018–1021 (2020).
29. C. W. Hsu, B. Zhen, A. D. Stone, and J. D. Joannopoulos, "Bound states in the continuum," Nat Rev Mater **1**(9), 16048 (2016).
30. C. W. Hsu, B. Zhen, J. Lee, and S. L. Chua, "Observation of trapped light within the radiation continuum," Nature **499**(7457), 188–191 (2013).
31. B. Zhen, C. W. Hsu, L. Lu, A. D. Stone, and M. Soljacic, "Topological nature of optical bound states in the continuum," Phys. Rev. Lett. **113**(25), 257401 (2014).
32. Z. Bomzon, G. Biener, V. Kleiner, and E. Hasman, "Space-variant Pancharatnam-Berry phase optical elements with computer-generated subwavelength gratings," Opt. Lett. **27**(13), 1141–1143 (2002).